Macromolecules
ARTICLE

Macromolecules **2010**, *43*, 543–552 **543**
DOI: 10.1021/ma9020467

Correlations between Morphologies and Photovoltaic Properties of Rod−Coil Block Copolymers

Manas Shah and Venkat Ganesan*

Department of Chemical Engineering, University of Texas at Austin, Austin, Texas 78712

Received September 14, 2009; Revised Manuscript Received November 5, 2009

ABSTRACT: We present results obtained using a drift-diffusion model for the structure−property correlations in photovoltaic devices based on self-assembly of rod−coil block copolymers. We use a self-consistent field theory model to generate the self-assembly morphologies of rod−coil block copolymers in confined situations. The density and orientational order parameter profiles so-obtained are then used as input to a recently proposed drift-diffusion model which predicts the photovoltaic device characteristics. The latter model allows for prescription of arbitrary morphologies of donor and acceptor phases while simultaneously incorporating the role of anisotropic charge transport of holes and excitons that arise in the ordered phases of rod−coil block copolymers. We present results elucidating the role of morphology of self-assembly, orientation of lamellar phases, domain widths, and the degree of phase separation and orientational ordering, upon the photovoltaic device characteristics.

I. Introduction

Photovoltaics and solar cells are emerging as attractive candidates for tapping into sources of renewable energy. Conventional solar cells based on crystalline silicon are highly efficient but are accompanied by the disadvantage of being expensive to fabricate.[1,2] Recently, polymeric and organic solar cells have emerged as attractive alternatives which are relatively inexpensive and allow fabrication onto flexible substrates using high throughput solution processing techniques.[1,2] However, presently, the best available polymer solar cells still lag behind that of conventional silicon devices in their efficiencies, and hence there is a need to understand the relationship between microstructure of such polymeric devices and their final properties to facilitate the design of efficient polymer photovoltaic devices.

There are many key issues regarding the design of polymeric photovoltaic (PV) devices which need to be addressed. We note that the mechanism of photovoltaic operation in polymer solar cells is different compared to conventional solar cells. Conjugated (or semiconducting) polymers are electronically active because of their highly polarizable π-electrons.[2] However, while in silicon devices photon absorption leads to the generation of free charge carriers (electrons and holes), in contrast, in conjugated polymers bound electron−hole pairs known as *excitons* are generated.[1−3] These pairs are bound together by a high Coulombic binding energy (relative to inorganic materials) of the order of 0.1−1.4 eV.[2] Such excitons can dissociate into electron and hole pairs at an interface between two materials having different electron affinities, thereby necessitating at least two chemical components in the fabrication of polymeric electronic devices.[1,4] The material with higher electron affinity is conventionally termed the acceptor (A), while the material with lower electron affinity is called the donor (D). The transport of the electrons and the holes to the respective electrodes constitutes useful power generated from the system. The latter transport process competes with a possibility for the electron−hole pairs to recombine as well as the decay of the original exciton after diffusion over a decay length.[1,2] It is evident then that an optimal length scale of phase separation between the two components may be required to balance the preceding transport processes in order to obtain high photocurrents.[5,6] Not surprisingly, understanding and controlling the distribution of the donor−acceptor interface within the device is an actively pursued strategy to improve the efficiency of the PV device.[7,8]

From the above discussion it is evident that the simplest device structures one might envision, viz., a bilayer device (or planar heterojunction) of a layer of donor and acceptor materials sandwiched between two electrodes, is not expected to be very efficient as PV device.[4,9,10] Indeed, due to the exciton decay process mentioned above, only excitons generated within a layer of ∼10 nm from the D−A interface can contribute to generation of charge carriers. Hence, the active layer region in such bilayer devices is small compared to the typical device thickness (which is of the order of 100−500 nm).[1,11,12] Consequently, most organic PV efforts focus on bulk heterojunction devices (BHJ) where interfaces between donor and acceptor material are distributed throughout the device.[1] In such a case, achieving donor and acceptor domains with a length scale of ∼10 nm would ensure that almost all photogenerated excitons diffuse to interface and dissociate to form free charge carriers (electrons and holes). This reasoning has motivated researchers to exploit thermodynamic phase separation of two chemically incompatible components as a potential route to achieve BHJ devices. The most common materials that have been studied in this context are blends of conjugated polymer such as poly(phenylenevinylene) (PPV) or poly(3-hexylthiophene) (P3HT) acting as donors mixed with either fullerene derivatives like (6,6)-phenyl C61-butyric acid methyl ester (PCBM) or inorganic materials like CdSe or titania acting as electron acceptors.[13−17] In these materials, efficiencies in the range 4−5% have been demonstrated, rendering them competitive with silicon solar cells.[1,14]

A potential issue with using donor−acceptor blends for the above applications is that the intermixing between the two components leads to *macrophase* separation. In such a case, the domain sizes are larger and due to kinetic effects may form dead ends and bottlenecks which prevent the transfer of charges to

*Corresponding author. E-mail: venkat@che.utexas.edu.

Published on Web 12/07/2009

appropriate electrodes. Consequently, it is harder to exercise complete control over the resulting morphologies and domain sizes. Not surprisingly, a number of physical parameters which typically modulate the kinetics of the phase separation processes, such as the choice of casting solvent, have been shown to play an important role in the efficiency of the resulting device.[14] Consequently, there is a need for ordered heterojunctions where the length scale for phase separation is controllable and smaller and in which continuous pathways exist for the charge carriers to reach the appropriate electrodes.[1,12]

Recently, semiconducting *block copolymers* have emerged as a promising alternative which can avoid the shortcomings noted in the context of blends.[12,18−22] Most such block copolymers consist of a conjugated polymer (donor), typically rodlike in conformation, linked to a flexible coil block. The flexible block is usually functionalized by electron-accepting moieties such as fullerene (C_{60}) or oxadiazole molecules.[18,23] Because of the chemical incompatibility between the two blocks, the block copolymers *microphase* separate into *equilibrium* ordered heterojunction structures which can potentially alleviate the kinetic issues noted in blends. Indeed, experiments have shown that the donor−acceptor block copolymer may actually exhibit enhanced photovoltaic efficiency relative to a blend of its individual polymers.[18,19]

Success in the above efforts requires a fundamental understanding of the self-assembly morphologies in rod−coil block copolymers under confinement (mimicking device conditions) and the correlations between the structure and the device properties. The morphological aspects of self-assembly of rod−coil block copolymers have been studied extensively in a number of theoretical[24−26] and experimental researches.[27−29] Some of the unique morphological features observed experimentally for rod−coil diblock copolymers that are not seen for flexible block copolymers include zigzag,[27] wavy lamellar,[27] arrowhead phases,[27] stripe, and puck phases.[28,30] In our earlier work, we developed a self-consistent field theory (SCFT) model for predicting the self-assembly morphologies of rod−coil block copolymers.[24] We delineated a morphological phase diagram within the context of two-dimensional phases which included smectic A and smectic C lamellar phases and hockey-puck-like cylindrical phases. Subsequent experiments of Segalman and co-workers have examined the phase diagram of rod−coil block copolymers systematically and have confirmed many of the predictions of the theory.[29,31] More recently, we have extended the preceding framework to address the effect of confinement on the self-assembly morphologies. In the latter work, we confirmed the existence of equilibrium self-assembly morphologies similar to bulk systems, with an additional possibility of the lamella phases being oriented either parallel or perpendicular to the confining surfaces depending on the interaction of the different blocks with the surfaces.[32]

In this article, we seek to extend our above researches on *morphology* predictions to address the *property* characteristics of PV devices consisting of rod−coil block copolymers. For this purpose, we adapt a continuum formalism termed the drift-diffusion model which characterizes the transport of excitons, electrons, and holes under photoadsorption to render predictions regarding the device characteristics. Such drift-diffusion models have been utilized in earlier researches to study the photovoltaic properties of bilayer devices[10] and bulk heterojunctions.[33] Most pertinent to the present article, in a seminal work, Buxton and Clarke used such a framework to study the device characteristics of thin film morphologies of *flexible* block copolymers.[12]

In this work, we extend the above researches by focusing on following aspects:

(i) Incorporating features inherent to the *semirigid or rodlike* nature of most of the donor molecules used in the experimental studies: Specifically, the nature of charge transport in such semirigid conjugated polymers is expected to be anisotropic.[1,34] Indeed, experimental evidence exists to show that the transfer of electronic excitation energy is predominantly intrachain (along the length of polymer backbone) as compared to interchain (hopping between different polymers) in the extended conformations of conjugated polymers.[35,36] Manifestations of this feature have been observed indirectly in experiments which have shown that an increase in crystallinity (concomitant with an increase in the orientational ordering of the chains) of conjugated polymer P3HT chains leads to increase in photocurrent.[37,38] Another set of experimental studies have shown that the hole mobility is enhanced when polymer is infiltrated into titania nanopores due to the alignment of polymer chains in the charge transport direction.[34] In the context of thin film field-effect transistors, Siringhaus et al. observed that mobility of charge carriers can vary by a factor of 100 depending on the nature of orientation of P3HT crystalline lamellae inside the film.[39] Also, Kinder et al. observed that intrachain hole mobility along polymer backbone was higher by a factor of 6.5 than the perpendicular direction in thin film transistors.[40] Quantum mechanical calculations have confirmed that while the charge transport in the interchain direction due to $\pi-\pi$ stacking of crystalline chains (of P3HT) can contribute to charge transport, this contribution is less dominant than the one in the intrachain direction (along polymer backbone).[41]

Motivated by the above results, in a recent article we proposed an extension of the drift-diffusion models to account for the possible anisotropy in mobility of holes and excitons. In the formalism we proposed, we modeled the anisotropy effect by rendering the mobility of holes and excitons to be anisotropic tensors whose values are determined by the average orientational order parameter of the rodlike donor molecules. Subsequently, by using several "simulated" model morphologies, we demonstrated that the anisotropy effect can have important consequences in determining the PV device characteristics. In the present article, we elaborate the details of our model and simultaneously adapt it to study the device properties of rod−coil block copolymers. We present the model details and the relevant parameters in section II.

As an aside we note that our drift-diffusion model is not restricted to block copolymers and in general accommodates the characteristics of BHJ devices with a continuous spatial variation of the morphologies and orientations of donor and acceptors and wherein the donor phases are assumed to be characterized by anisotropic hole and exciton mobilities. In fact, in different sections we consider several "simulated" morphologies to understand the physics underlying the results for rod−coil block copolymers.

(ii) We use morphologies generated from a SCFT model of rod−coil block copolymers under confinement to study their device characteristics. While a description of SCFT model and a discussion of the morphological phase diagram (for confined systems) is presented in a different article,[32] the results in this section demonstrate that the device characteristics of realistic systems employing donor−acceptor materials of rod−coil block copolymers involve a complex interplay of several features including the orientation of domains, domain widths, the degree of phase separation, and the orientation of rodlike domain molecules in influencing the PV characteristics of the device.

The rest of the article is arranged as follows: In section II, we elucidate the key features of the drift-diffusion model to study the photovoltaic characteristics of devices based on self-assembly of rod−coil block copolymers. In section III, we provide results for photovoltaic properties of different morphologies exhibited by rod−coil block copolymers. We also discuss the role of domain

widths, degree of phase separation, thickness of device, and anisotropy in charge transport on photovoltaic properties.

II. Drift-Diffusion Modeling of Device Characteristics

A. Model. In this section, we present the formalism used to study the device characteristics of photovoltaic cells. The model we employ falls in the general category of drift-diffusion models, which captures within a continuum reaction−diffusion framework the generation of excitons, their dissociation into electrons and holes, and the subsequent transport of electrons and holes to the electrodes. Drift-diffusion models yield the spatial variation of electric field and densities of electrons, holes and excitons.[3,42] Below, we present our adaptation of such a formalism to incorporate (i) the anisotropic mobility of charge carriers and (ii) the morphologies resulting from SCFT calculations. The former aspect constituted the focus of an earlier short communication article.[43] Below, we elaborate on the details of the model and the parameters used in its solution. Subsequently, we discuss the numerical methods used to solve the resulting equations.

The drift-diffusion model consists of the following equations governing the exciton (x), electron (n), and hole (p) concentrations and the electrostatic potential (ψ):[3,12,42]

$$\frac{\partial x}{\partial t} = \frac{1}{q}\nabla\cdot[k_B T \mu_x \cdot \nabla x] + G(\mathbf{r}) - R_d(x) - D(\mathbf{E}, x) + \frac{1}{4}R(n,p) \tag{1}$$

$$\frac{\partial n}{\partial t} = \frac{1}{q}\nabla\cdot\mathbf{J}_n + D(\mathbf{E}, x) - R(n,p) \tag{2}$$

$$\frac{\partial p}{\partial t} = -\frac{1}{q}\nabla\cdot\mathbf{J}_p + D(\mathbf{E}, x) - R(n,p) \tag{3}$$

$$\nabla.(\epsilon\nabla\psi) = -q(p-n) \tag{4}$$

Equations 1−3 represent continuity equations for exciton, electron, and hole concentrations. Equation 4 represents the Poisson's equation relating the electrostatic potential (ψ) to the local difference in concentrations of electrons (n) and holes (p). ϵ denotes the permittivity of the medium, and q denotes the unit of elementary charge.

In eq 1, the first term represents the transport due to diffusion of excitons and the mobility coefficient is denoted as $\boldsymbol{\mu}_x$. The terms $R_d(x)$, $G(\mathbf{r})$, and $D(\mathbf{E},x)$ represent respectively the rates of decay, photogeneration, and dissociation of excitons. The functional forms for these rates are assumed to be similar to those adopted in earlier works.[3,10,12] To maintain completeness, we present a brief compendium of the relevant equations below. The decay rate of excitons $R_d(x)$ is assumed to be of the form $R_d(x) = x/\tau_x$, where τ_x is the average lifetime of exciton chosen such that the diffusion length of exciton is 10 nm. The term $G(\mathbf{r})$ is assumed to be of the form

$$G(\mathbf{r}) = \sum_i \Phi_i(\nu_i)\alpha_i(\nu_i)\exp[-\alpha_i(\Delta - y)] \tag{5}$$

where $\Phi_i(\nu_i)$ represents the frequency (ν_i) dependent incident photon flux.[44] The incident power is obtained by summing over the intensities at different frequencies. The frequency dependent absorption coefficient (α_i) is assumed to have a Gaussian distribution as a function of the frequency, ν_i.[3,12] The photogeneration of excitons have been assumed to have an exponential dependence on the distance from the transparent top electrode, $(\Delta - y)$.[3,12]

The dissociation of excitons $D(\mathbf{E},x)$ is modeled through Onsager's theory of electrolyte dissociation[45]

$$D(\mathbf{E}, x) = xN_f \int_0^\infty k_D(\mathbf{E}, a)F(a)\,da \tag{6}$$

where k_D is the electric field dependent rate constant given by Braun:[46]

$$k_D(\mathbf{E}, a) = K_R \frac{3}{4\pi a^3}\exp(-E_{b0}/k_B T)\left[1 + b + \frac{b^2}{3} + \frac{b^3}{18} + \frac{b^4}{180} + ...\right] \tag{7}$$

with

$$K_R = q\mu_{avg}/\epsilon \tag{8}$$

$$b = q^3|\mathbf{E}|/8\pi\epsilon k_B{}^2 T^2 \tag{9}$$

where μ_{avg} is the averaged mobilities of electrons and holes at that point in space. The dissociation rate is integrated over a Gaussian distribution of separation distances (a), specified by $F(a)$. The exciton binding energy is denoted as E_{b0}. The term $R(n,p)$ represents the recombination rate of electrons and holes which is assumed to be a bimolecular reaction described by a Langevin recombination term. Only a fraction (1/4) of electrons and holes are assumed to recombine to form singlet excitons.[47]

$$R(n,p) = q(\mu_n + \mu_p)pn/\epsilon \tag{10}$$

where μ_n and μ_p represent the mobilities of electron and holes, respectively.

In eqs 2 and 3, the first term represents the flux (current density) of the charge carriers which are assumed to be of the form

$$\mathbf{J}_n = -qn\boldsymbol{\mu}_n\cdot\nabla\psi + k_B T\boldsymbol{\mu}_n\cdot\nabla n \tag{11}$$

$$\mathbf{J}_p = -qp\boldsymbol{\mu}_p\cdot\nabla\psi - k_B T\boldsymbol{\mu}_p\cdot\nabla p \tag{12}$$

In the above, the mobilities of electrons and holes are denoted by $\boldsymbol{\mu}_n$ and $\boldsymbol{\mu}_p$, respectively. The above fluxes can be seen to consist of two contributions: a diffusive flux arising from the concentration gradient and a drift term arising from the influence of electric field (since exciton is neutral, eq 1 does not have a drift term). Prior researches which have used the above formalism have assumed that the (electric-field-dependent) mobilities $\boldsymbol{\mu}_i (i = n, p)$ are isotropic and are given by the Poole−Frenkel form

$$\mu_i = \mu_i^0 \exp(\gamma\sqrt{|\mathbf{E}|})\mathbf{I} \tag{13}$$

where μ_i^0 is the zero field mobility and the field-dependent mobility parameter is represented by γ.

To adapt the above formalism to the systems of interest in this article, a few modifications are needed. On the one hand, the above equations need to be recast in a form which accounts for the input spatial morphologies of the donor−acceptor system. In the present work, we assume the morphologies are characterized by the fields which denote the volume fraction profiles of the donor ($\phi_D(\mathbf{r})$) and acceptor ($\phi_A(\mathbf{r})$). Most polymeric systems are assumed to be incompressible, where the constraint $\phi_D(\mathbf{r}) + \phi_A(\mathbf{r}) = 1$ holds. In the systems of interest in this article, the exciton undergoes dissociation at the donor−acceptor interface, where the binding energy is reduced by the difference in electron affinities of the two materials.

A second feature relates to the issue discussed in the Introduction that experimental evidence points to the fact that the mobilities of holes and excitons not only depend on the spatially varying density profiles and electric fields but also are expected to be anisotropic and in general different along the backbone of the donors compared to perpendicular to it. To account for the latter feature, we generalize the above function forms (eq 13) to allow the mobilities $\boldsymbol{\mu}_x$ and $\boldsymbol{\mu}_p$ to be anisotropic tensors which depend on the average state of orientation of the rods. We further assume that the information regarding the average state of orientation of the rods is available (as output of a morphological model) and characterized by an orientational order parameter $\mathbf{S}(\mathbf{r})$.[24,48,49] The *magnitude* of orientational order parameter ($S(\mathbf{r})$) is obtained by evaluating the maximum eigenvalue of the tensorial order parameter.

To illustrate the above modifications, we explain how the hole mobility is influenced by the density variations and orientational ordering of one of the species. Explicitly, the hole mobility is assumed to be of the form

$$\boldsymbol{\mu}_p(\mathbf{r}) = \mu_p^I(\mathbf{r})\mathbf{I} + \mu_p^S(\mathbf{r})\mathbf{S}(\mathbf{r}) \tag{14}$$

where μ_p^I and μ_p^S denote the isotropic and anisotropic term, respectively, and $\mathbf{I}$ denotes the identity matrix. The coefficients $\mu_p^I(\mathbf{r})$ and $\mu_p^S(\mathbf{r})$ (in eq 14) are in turn assumed to be dependent on the volume fractions of the donor and acceptor species as

$$\mu_p^j(\mathbf{r}) = \mu_{p\mathrm{A}}^j(\mathbf{E})\phi_A(\mathbf{r}) + \mu_{p\mathrm{D}}^j(\mathbf{E})\phi_D(\mathbf{r}) \quad (j = I, S) \tag{15}$$

Each of the above coefficients $\mu_{p\mathrm{A}}^j$ and $\mu_{p\mathrm{D}}^j$ are in turn assumed to be of the Poole−Frenkel form (eq 13). We note that the above assumption for volume fraction dependence is valid for the extreme cases of pure phases and phase mixed cases, and hence the linear relation of mobility coefficients is akin to a simplistic ideal gas mixing rule. Unfortunately, at the level of our modeling, we cannot prove this relationship and hence adopt it as the simplest possible one among a class of mixing rules. We quantify the anisotropy in the mobility of the holes by a single parameter

$$\mu_R = \mu_p^{S0}/\mu_{p\mathrm{D}}^{I0} \tag{16}$$

where the "0" superscript indicates zero-field mobilities (eq 13).

The above generalized drift-diffusion formalism allows us to account for spatially varying morphologies and the anisotropy in charge transport within an internally consistent framework for donor−acceptor mixtures characterized by a continuous spatial variation of the morphologies of donor and acceptors, with the donor phases assumed to be characterized by anisotropic hole and exciton mobilities. We emphasize that the above model only requires as input the volume fraction profiles and the orientational order parameter in the donor phase and accommodates both donor−acceptor blends and block copolymers. We believe our model is a significant improvement over previous models and allows us to account for the effects of orientation and (potentially) crystallization of donors in prediction of photovoltaic properties. As noted in the Introduction, Buxton and Clarke introduced a formalism for flexible block copolymers which in many respects is similar except in not incorporating the effects of anisotropic mobility.[12] Since not all equations were detailed in their article, we are unable to present a detailed comparison of the functional forms they used to modify their equations to account for compositional inhomogeneities.

The output of the above equations are the spatially varying electron, hole, exciton densities, the fluxes of electrons, holes, and excitons, and the electrostatic potentials. The photovoltaic response is measured in terms of a current−voltage ($J-V$) curve. The total current density ($\mathbf{J} = \mathbf{J}_n + \mathbf{J}_p$) comprising both electron and hole current density is evaluated as a function of applied voltage (V) between the two electrodes. The quantities typically of interest are (i) the short-circuit current (J_{SC}) which is obtained at zero voltage condition and is the maximum current obtainable from the solar cell and (ii) open-circuit voltage V_{OC} which is the condition where the output current is zero and represents the maximum voltage obtainable from the solar cell. The photovoltaic efficiency is given by: $-\eta = (JV)_{max}/P_{in}$, where P_{in} is the input power of photons and $(JV)_{max}$ is maximum power obtainable from the device. High values of J_{SC} and V_{OC} are desirable for efficient solar cell devices. In our results, the open-circuit voltage (V_{OC}) was observed to not change significantly (a result which is consistent with the fact that the V_{OC} is strongly dependent on the electrode characteristics). Hence, all our subsequent results are discussed in terms of short-circuit current (J_{SC}) only.

B. Boundary Conditions and Numerical Details. The above equations (eqs 1−4) are supplemented by boundary conditions for charges at the electrodes. We adopt the thermionic injection and recombination models used in previous researches in this context.[10,50,51] The drift-diffusion equations are numerically discretized using Scharfetter−Gummel scheme.[52] The conjugate gradient method is used to evolve the Poisson's equation while the Crank−Nicholson method is used to obtain electron, hole, and exciton densities at each new time step.[53] The spatial discretization used is 1 nm.

C. Parameters. The model detailed in the previous section involves a number of parameters. In this work, we fixed most of the device parameters and mainly focus on the interplay between morphologies, anisotropic mobilities, and device characteristics. Most of the following parameters have been taken from the paper of Buxton and Clarke.[12] The zero field mobilities of electron in acceptor and donor regions are taken to be 1×10^{-8} and 1×10^{-11} $m^2\ V^{-1}\ s^{-1}$, respectively ($\mu_{n\mathrm{A}}^0$ and $\mu_{n\mathrm{D}}^0$). The zero field mobilities of holes in the donor and acceptor regions are taken to be 1×10^{-8} and 1×10^{-11} $m^2\ V^{-1}\ s^{-1}$, respectively ($\mu_{p\mathrm{D}}^0$ and $\mu_{p\mathrm{A}}^0$). The exciton mobility, μ_x, is fixed at 3.86×10^{-9} $m^2\ V^{-1}\ s^{-1}$ and has a lifetime, τ_x, of 1 μs, unless otherwise stated. The field dependent mobility parameter is taken to be $\gamma = 5 \times 10^{-4}$ $m^{1/2}\ V^{-1/2}$ (eq 13). The exciton binding energy is taken to be 0.5 eV, and the Schottky barrier height for injection of charge carriers is taken to be 0.5 eV. The built-in voltage is assumed to be 0.5 V.[12]

D. SCFT Model for Donor−Acceptor Morphologies. To model the self-assembly of confined rod−coil block copolymers, we use the model of Pryamitsyn and Ganesan[24] which

utilizes self-consistent field theory (SCFT) to model the self-assembly of rod−coil block copolymers in the bulk. Along lines similar to the earlier work on flexible block copolymers,[54] we extended the model to incorporate the effects of confinement and surface interactions upon self-assembly. The details of our model and the resulting self-assembly behavior will be presented in a separate publication.[32]

Briefly, the key ingredients utilized in our SCFT model are the Flory−Huggins interactions to model the repulsive interactions between the rod and coil block, Gaussian stretching energy for the coil block, and Maier−Saupe potential to describe the orientational ordering between liquid crystalline rod molecules. The phase diagram in thin-films of rod−coil block copolymers is affected by volume fraction of one of the blocks (f), the Flory−Huggins interactions parameter (χN), the Maier−Saupe parameter (ωN), the size asymmetry ratio β, and the surface interactions.[24,28,29,55] We utilize this model to obtain the densities and orientational order parameters ($\phi_A(\mathbf{r})$, $\phi_D(\mathbf{r})$, and $\mathbf{S}(\mathbf{r})$) which are in turn utilized as input to our photovoltaic model. All the length scales in the SCFT model are normalized by radius of gyration of the coil block, R_g. For using these morphologies in our photovoltaic model, we use a conversion factor of $R_g = 3.33$ nm.

III. Results and Discussion

A. Influence of the Morphology of Self-Assembly upon Device Characteristics. In Figure 1a, we display two representative morphologies arising from the self-assembly of rod−coil block copolymers in confined situations. These are lamellar morphologies which are oriented parallel and perpendicular to the confining surfaces. The molecular parameters (χN, ωN, f, and β) for both parallel and perpendicular lamellae were kept the same. However, the case of perpendicular lamellae corresponds to the situation in which the confining surfaces had no preferential interactions with either of the polymers. In contrast, the parallel morphology was achieved for the case when the anode surface was assumed to prefer the rod (donor) phase, whereas the coil (acceptor) was favored at the cathode. In both the parallel and the perpendicular morphologies, the conditions were such that the rods were aligned perpendicular to the interface between rods and coils (smectic A morphology).

From Figure 1b, it is evident that the device having perpendicular lamellae ($\eta = 0.75\%$) exhibits better performance than parallel lamellar morphology ($\eta = 0.16\%$). Indeed, the perpendicular lamella phase benefits from several factors that are key for better performance of polymer solar cell devices. On the one hand, direct pathways exist for both electrons and holes to reach the respective electrodes. Moreover, since the rods are aligned perpendicular to the lamellar interface, the excitons are able to reach the D−A interface easily because of the preference for transport of excitons along the backbone of the donor molecules. In contrast, the device possessing parallel lamellae benefits only from the donor−acceptor microphase separation and the fact that rods are aligned perpendicular to the surface of electrodes. The latter furnishes higher charge transport rates for holes to travel to the anode. However, the major disadvantage of parallel lamellae is that the layers of donors (rod phase) and acceptors (coil phase) act as blocking layers for electrons and holes, respectively. Therefore, in parallel lamellae, the donor−acceptor interfaces closer to the electrodes contribute toward charge generation and photocurrent, whereas the charges generated at other interfaces are mostly blocked by the alternating donor−acceptor lamellaes.

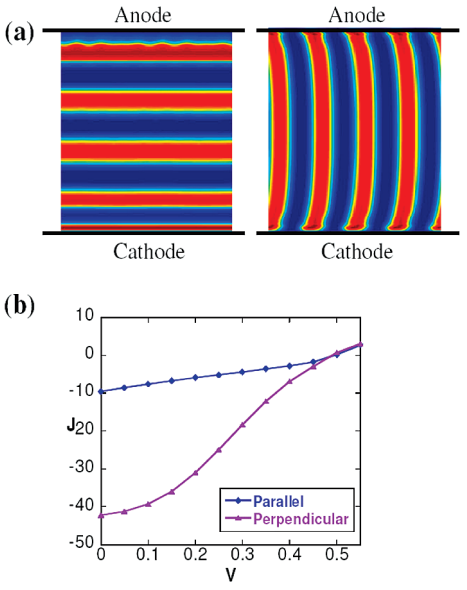

Figure 1. (a) Density profiles for donor and acceptor phases for parallel lamellae and perpendicular lamellae. The coil block is shown in red, and the rod block is shown in the blue phase. The parameters are $\chi N = 10$, $f = 0.40$, $\omega N = 30$, and $\beta = 6$. The anisotropy in charge transport is $\mu_R = 0.67$. (b) $J-V$ curves for the preceding phases. The units are A m^{-2} for current density (J) and volts for voltage (V).

In general, by carefully tuning the surface interactions and/or by applying external fields, it is possible to align the layers of block copolymers to be oriented parallel or perpendicular to the electrode interfaces. This raises the question, "in general, what is the role of the influence of orientation of the domains (relative to the electrodes) in influencing the device PV characteristics?" We note that in the example considered above these considerations were complicated by the occurrence of multiple domains (which act as blocking layers) and the presence of anisotropic charge transport. Of interest is the specific influence of the *orientation of the lamellae upon the PV device characteristics*.

To study the effect of domain orientation on photovoltaic properties, we considered two model morphologies. In Figure 2a, we show the schematics of parallel and perpendicular bilayer devices considered. To isolate the effects arising just from the orientation of the bilayers, we switch off the effects arising from the anisotropic mobilities (equivalently, we set $\mu_R = 0$ in eq 16). In Figure 2b, we display the $J-V$ curves for the two cases illustrated in Figure 2a. It is seen from the results that even for the case of a single donor−acceptor interface, having domains oriented perpendicular to the electrodes exhibits better performance relative to the parallel domains. Moreover, the reasoning discussed above is confirmed in the results for electron densities for parallel and perpendicular bilayers plotted in Figure 2. We observe in Figure 2c that there is a continuous generation of electrons (and equivalently holes) throughout the device in perpendicular domain orientation. Since more excitons can dissociate throughout the device, charges are generated throughout the device between the electrodes, and such a configuration leads to higher short-circuit current (J_{SC}). In contrast, in the parallel bilayer, only excitons generated within the exciton diffusion length scale of the donor−acceptor interface are seen to diffuse to the donor−acceptor interface and result in production of electrons and holes. Consequently, only a small fraction of photons get converted to charge carriers. With this reasoning, it

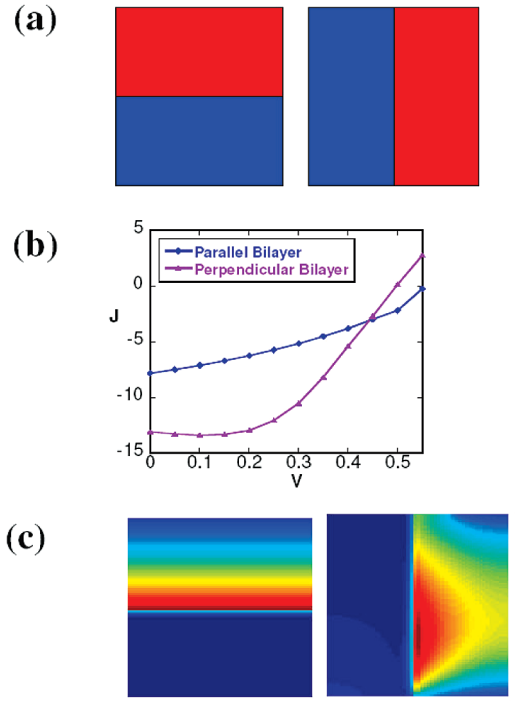

Figure 2. (a)Schematics for parallel bilayer and perpendicular bilayer morphology. The red phase is the acceptor layer, and blue layer is the donor phase. (b) Effect of domain orientation on the $J-V$ response. The units are A m^{-2} for current density (J) and volts for voltage (V). (c) Electron density (n) for parallel and perpendicular bilayer morphology. $V = 0.45$ V, $\Delta = 100$ nm.

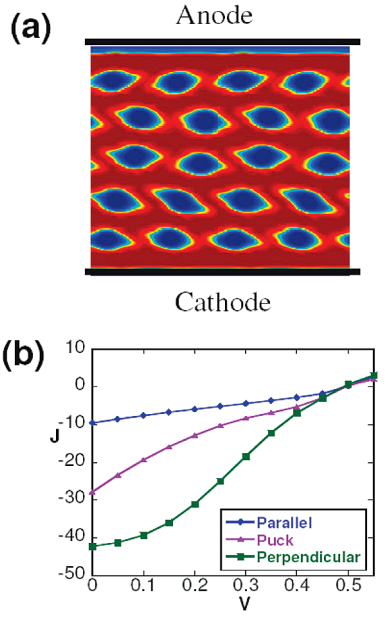

Figure 3. (a) Density profiles for donor and acceptor phases for puck phases. The parameters are $\chi N = 16, f = 0.6, \omega N = 64$, and $\beta = 10$. (b) $J-V$ curve for puck morphology compared with $J-V$ curves for parallel and perpendicular morphology. The units are A m^{-2} for current density (J) and volts for voltage (V).

is also evident that the efficacy of the parallel bilayer device would increase upon decreasing the thickness of the PV device.

We note that other "nonlayered" self-assembly morphologies are also possible in confined films of rod−coil block copolymers.[24,28] Figure 3 displays one such case termed the puck phase ($\eta = 0.31\%$) and compares its device characteristics to the parallel and perpendicular lamellar phases. The puck phase morphology is achieved in rod−coil block copolymers at high volume fractions of the coil block. In comparing the device characteristics of puck phases to the earlier-discussed lamellar morphologies, it is seen that the puck phases exhibit performance intermediate to parallel and perpendicular lamellae. Indeed, while puck phases offer the advantage of high interfacial area between rods and coil blocks, they suffer from the absence of continuous pathways for holes to reach the anodes. While the former facilitates exciton dissociation and leads to higher production of free charges, the latter hinders hole transport. Another interesting thing to note is that whereas $J-V$ curves for the lamellae are convex-shaped, the $J-V$ response for the puck phase morphology has a concave shape. This arises due to the presence of the acceptor phase at the anode which results in a buildup of electron charge at the wrong electrode. Such charge accumulation at organic layer−electrode interface has been documented to result in concave-shaped $J-V$ curve.[56,57] Recently, it has been shown in experiments in the context of rod−coil block copolymer solar cells that cylindrical nanostructures aligned parallel to the confining surfaces[7] were less efficient relative to other morphologies. Our results are consistent with these experimental observations.

In summary, our analysis suggests that for efficient charge transport and efficiencies the donor and acceptor phases should have continuous nanochannels between the two electrodes. For the same reason, lamellar morphologies observed in rod−coil block copolymers exhibit more desirable characteristics than the nonlamellar morphologies in dispersed phases like puck phases. In all our results, the open-circuit voltage (V_{OC}) was observed to not change significantly. Hence, all our subsequent results are discussed in terms of short-circuit current (J_{SC}) only.

B. Effect of Domain Sizes. Donor−acceptor block copolymers offer unique advantages in the ability to control the domain sizes resulting from self-assembly. Indeed, this is most easily accomplished by either using longer block copolymers and/or mixing with a third component. In contrast, the domain sizes achieved in *blends* of donors and acceptors tend to be much larger and usually controlled by the kinetics of the phase separation process. These considerations motivate the question, "what is the influence of the domain sizes upon the PV device characteristics?" Specifically, of interest is whether there is an "optimum" domain size for achieving the best PV device characteristics.

At the outset, we address the above issue in the context of morphologies of rod−coil block copolymers. One possible means to modulate the domain sizes in rod−coil block copolymers is to vary the size asymmetry ratio β. β is a nondimensional parameter quantifying the length of the rod unit. In the case of smectic A morphology formed by the rod−coil block copolymers, the domain width is directly proportional to the value of β.[24] In Figure 4, we plot $|J_{SC}|$ as a function of the β parameter. To isolate the effects arising from the domain widths, the displayed device characteristics were specifically computed within the framework of the isotropic transport model ($\mu_R = 0$). We observe that the short-circuit current correlates inversely with the length of the donor units and the thickness of the domains. Smaller rod units facilitate more interfaces between the rod and coil phases and in turn leads to enhanced production of electrons and holes. The overall behavior is governed by higher exciton capture due to presence of more number of interfaces. In the perpendicularly oriented lamellae, these charge carriers have direct access to the electrodes and therefore enhance the overall efficiency of the PV device.

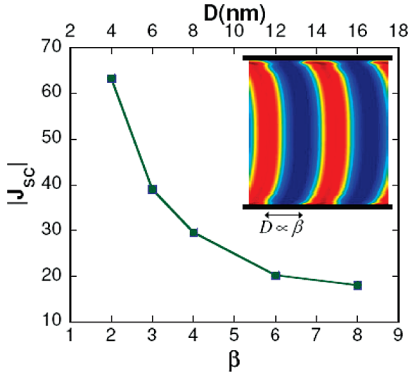

Figure 4. Effect of domain spacing for rod−coil block copolymers on the short-circuit current. The units are A m^{-2} for short-circuit current density (J_{SC}).

The above-noted increase in J_{SC} cannot continue indefinitely to very small domain spacings. Indeed, at very small domain widths, there is an unfavorable propensity of electrons and holes to undergo recombination and reduce the efficiency. An optimal condition is expected to be realized when the interfaces are spaced far enough to diminish the recombination effect, but while the interfaces are close enough to capture most of the excitons being generated. Consequently, with increasing *decay length of the excitons* the "optimal" domain width at which highest J_{SC} is achieved is expected to manifest at larger domain spacings. To verify this reasoning, we considered simulated morphologies with prescribed domain widths to explore the interplay between recombination rates, domain widths, and exciton decay. A schematic of such perpendicular multilayer morphology is shown in Figure 5a. In Figure 5b, we display the J_{SC} values of as a function of both the domain widths and the exciton lifetimes (τ_x). Note that the exciton diffusion length scale l_D is related to the exciton lifetimes τ_x through $l_D \sim \sqrt{\tau_x}$. We observe that indeed for the smallest values of τ_x the results are very similar to those presented in Figure 4, with J_{SC} monotonically decreasing with increasing domain widths (the optimal domain width is at much smaller domain thicknesses and is not within the range of displayed results). However, for larger values of τ_x we observe that there is indeed an optimal width at which the highest photocurrent is achieved. Moreover, it is evident that the optimal domain widths increase with increasing τ_x, consistent with our above reasoning that the optimal domain widths should scale with the exciton diffusion length scales.

The above results point to an interesting design guideline that to extract the optimal device characteristics, the donor−acceptor domains need to be of the order of the exciton diffusion lengths. Since the domain widths in the morphologies achievable in block copolymers typically fall in this range (and can be tuned by tuning the physicochemical features of the polymer), block copolymers may prove especially attractive in the fabrication of organic photovoltaics. We also note that the above results are consistent with Monte Carlo simulations that an optimal range of phase separation is needed for efficient device due to competition between the exciton dissociation and efficient charge separation.[5] In the same research, it was also observed that optimal domain width increased upon increasing the exciton lifetimes.[5]

C. Effect of Chemical Incompatibility and Degree of Phase Separation. The chemical incompatibility between the donor and acceptor phases is another design parameter which can be modulated by choosing alternative combinations of

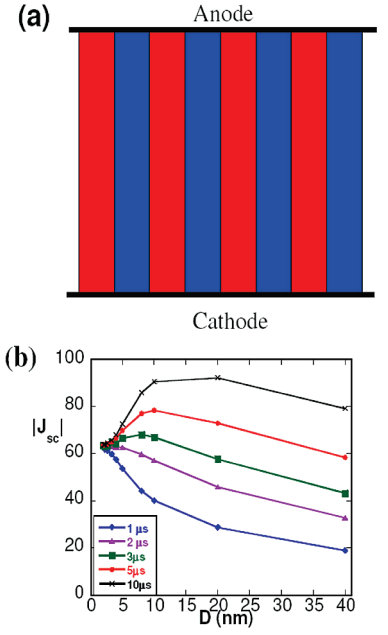

Figure 5. (a) Schematic of perpendicular multilayer morphology. (b) Effect of domain spacing for different exciton lifetimes. The units are A m^{-2} for short-circuit current density (J_{SC}).

donors and acceptors. Chemical incompatibility in turn determines features such as the degree of phase separation and the domain size and also governs the nature of interfacial widths between the donor and acceptor. In our model, the chemical incompatibility between the two blocks of the block copolymer is embodied in the Flory−Huggins interaction parameter (χN). In this section, we present results for the device characteristics for different χN. To maintain the focus on the issue of interest, we use the isotropic transport version of our model.

In Figure, 6, we display the $J-V$ curves for different values of χN. The conditions $\chi N = 6$ and 8 correspond to systems which are not microphase separated (as seen from the uniform density profiles for $\chi N = 8$ in Figure 6a), whereas for conditions such that $\chi N \geq 12$ the system is observed to be microphase separated and exhibits perpendicular lamellar morphology under confinement. Correspondingly, a jump in photocurrent device characteristics is observed when the block copolymer undergoes microphase separation. Increasing χN beyond the microphase separation transition is seen (Figure 6b) to enhance the efficiency of the PV device.

The above results can be rationalized on the basis of two effects evident in the density profiles for different χNs (Figure 6a). Higher χN is seen to correlate to more strongly segregated donor and acceptor phases. In turn, this results in improved transport properties for holes in the donor (rod) phase and electrons in the acceptor (coil) phase. A second effect evident is that increasing the chemical incompatibility results in a reduction of the interfacial width. This is seen explicitly in Figure 6c, which displays the variation of interfacial width (ξ) as a function of the degree of phase separation (χN). Smaller interfacial widths would facilitate better charge separation by reducing the propensity for recombination between electrons and holes and thereby increase the short circuit current. The increased segregation and the reduced interfacial widths are expected to act in unison to result in better overall transport and device characteristics with increasing chemical incompatibility.

The above results were seen to involve the synergistic action of two distinct features. To further test our hypothesis

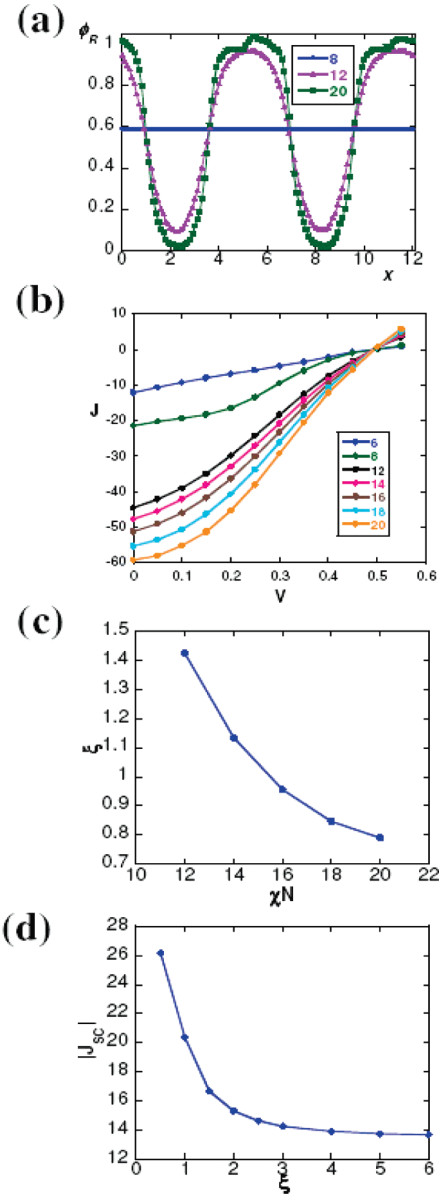

Figure 6. (a) Rod density profiles for $\chi N = 8$, $\chi N = 12$, and $\chi N = 20$. Well microphase separated lamellaes are observed for higher χN value. (b) $J-V$ curves for different values of phase separation characterized by χN. Higher degree of segregation implies thinner interfaces which leads to low values of recombination and efficient charge separation at interface. The units are A m^{-2} for current density (J) and volts for voltage (V). (c) Interfacial width ξ obtained as the full width at half-maximum of peaks in the product of densities of acceptor and donor phases, $\phi_A(\mathbf{r}) \times \phi_A(\mathbf{r})$. (d) Relationship between J_{SC} and ξ (nm) for artificial perpendicular bilayer morphology.

specific to the correlation between the photovoltaic properties and the interfacial width, we utilized a perpendicular bilayer morphology (depicted in Figure 2a) and varied the interfacial width of the donor−acceptor interface. The variation of J_{SC} as a function of the interfacial width for this simulated morphology is displayed in Figure 6d and confirms that reducing interfacial width indeed improves the photovoltaic properties. These results are also consistent with experimental observations which have demonstrated that solvents leading to better phase separation yields higher short-circuit current and hence higher photovoltaic efficiencies.[14]

D. Influence of Anisotropic Charge Transport Characteristics. In this section, we consider the interplay between the

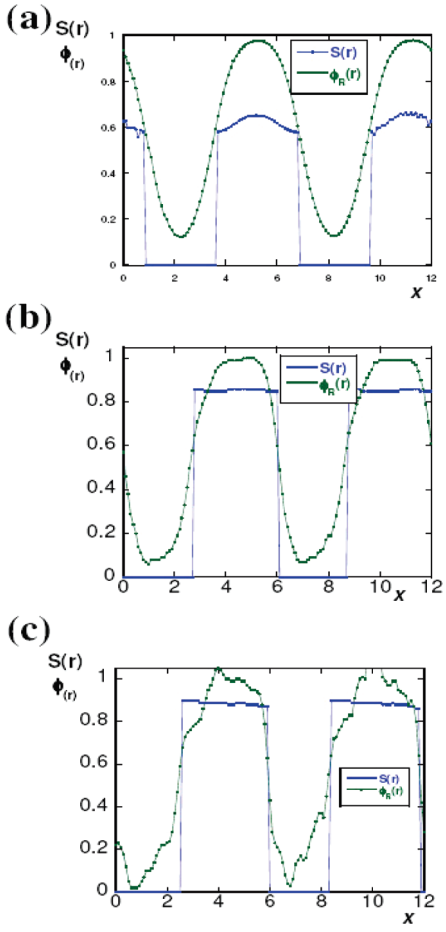

Figure 7. One-dimensional density profiles of orientational order parameter ($S(\mathbf{r})$) and rod density ($\phi_R(\mathbf{r})$) for three values of ωN: (a) 15, (b) 40, and (c) 100.

anisotropic charge transport characteristics and the orientation of the donor units in the different self-assembled morphologies. We note that in our SCFT model for rod−coil block copolymers the propensity for orientational ordering arises through a Maier−Saupe orientational interaction term whose strength is quantified by the parameter ωN. To explore the influence of the *degree of orientational ordering* upon the device characteristics, we consider perpendicularly oriented lamellar morphologies generated with three different values of ωN.[24] In Figure 7, we display the orientational order parameters ($S(\mathbf{r})$) and the rod density profiles ($\phi_R(\mathbf{r})$) for three values of ωN considered for probing the device characteristics. $\omega N \approx 15$ corresponds to the onset of orientational ordering. In Figure 8, we plot the variation of absolute value of short-circuit current (J_{SC}) as a function of the anisotropy parameter μ_R for the three situations depicted in Figure 7. Near the isotropic−smectic transition ($\omega N \approx 15$, where $S \approx 0.6$), the short-circuit current is seen to increase monotonically with increasing anisotropy in the mobility. On the other hand, for larger values of the Maier−Saupe parameter ωN (where the nematic order parameter $S > 0.9$), there is seen to be an optimal value of anisotropy (measured by μ_R) for which J_{SC} is a maximum.

To rationalize the above results, we note that in the perpendicular lamellae considered in this section the rods are aligned parallel to the confining surfaces. Increasing μ_R increases the mobility along the polymer backbone (intrachain) and reduces the mobility along the perpendicular (interchain) direction (refer to eq 14). As the mobility of

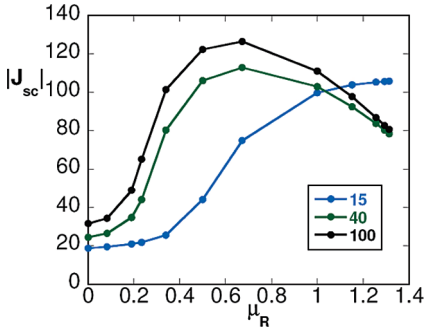

Figure 8. Effect of anisotropic mobility and orientational ordering on photocurrent.

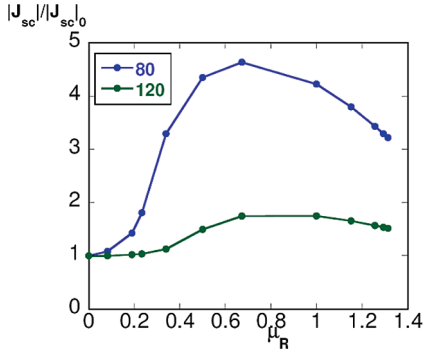

Figure 9. Effect of anisotropic mobility on photocurrent for two different thickness, 80 and 120 nm. $\omega N = 40$.

holes and excitons is rendered more anisotropic, the rate of excitons traveling to donor−acceptor interface and the subsequent charge separation improves. This is reflected in the larger efficiencies noted with initially increasing μ_R and for morphologies with better orientational ordering ($\omega N = 40, 100$). However, the preceding effects are concomitantly accompanied by a reduction in the transport of holes to the anode (in the interchain direction). At large μ_R, the interchain transport to the anode becomes the rate limiting step, leading to a lowering of the efficiency. It is evident that the competition between the transport in the parallel and perpendicular directions should depend on the magnitudes of both μ_R and S (cf. eq 14). Not surprisingly, in morphologies with pronounced orientational ordering, the optimal μ_R occurs at a smaller value relative to morphologies which are less ordered.

Since the above reasoning invokes transport to the electrodes as one competing factor, in situations where anisotropy is relevant, the thickness of the device is expected to play an important role in determining the device characteristics. In Figure 9, we consider the effect of interplay of anisotropy and thickness of the device on the short-circuit current. We consider the case where the rods exhibit strong orientational ordering ($\omega N = 40$). We plot the value of short-circuit current normalized by value of J_{SC} at zero anisotropy ($\mu_R = 0$) as a function of the degree of anisotropy. It is observed that the short-circuit current is much higher for thinner device (80 nm) as compared to the thicker device (120 nm) for all values of μ_R considered. Indeed, the 80 nm device exhibits almost a 5-fold increase in short-circuit current at the optimal value of anisotropy ($\mu_R = 0.67$) compared to the value at zero anisotropy. Moreover, the nonmonotonicity in J_{SC} is seen to be much less pronounced for the case of larger thickness. These results can be rationalized by noting that the charge transport in larger films are

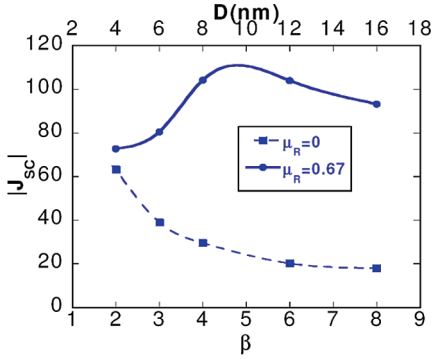

Figure 10. Effect of domain spacing for rod−coil block copolymers on the short-circuit current. The variation of $|J_{SC}|$ as a function of domain size is different for isotropic and anisotropic charge transport. The units of J_{SC} is A m^{-2}.

dictated mainly by the thickness of the film and the distance the charges have to travel to get to the respective electrodes. In thicker films, the increase in transport rates along intrachain direction is compensated by the related factors of the decrease in the interchain transport and the larger distance charges have to travel in a thick film. Therefore, the effect of anisotropic charge transport on photocurrent is much less pronounced for larger film thickness.

We now discuss the interplay of domain size effects with the anisotropic transport of charges and excitons (refer to Figure 10). For this, we considered the same morphologies used to generate Figure 4 but computed the device curves with $\mu_R = 0.67$ (for comparison, we also display the isotropic case, $\mu_R = 0$). Increasing the degree of anisotropy in charge and exciton transport is seen to improve the photovoltaic response compared to the case where the charge transport was assumed to be isotropic. Interestingly, we observe that for $\mu_R = 0.67$ there is an optimal domain width for which the short-circuit current is maximum. This contrasts with the situation for $\mu_R = 0$ where the short-circuit current continuously increased up to the smallest domain sizes we probed.

As discussed in an earlier section (sectionIII.B), the occurrence of an optimal domain width reflects an interplay between exciton dissociation and recombination. The inclusion of anisotropic charge transport characteristics tends to shift the optimal domain widths to higher values relative to the isotropic situation (for $\mu_R = 0$ the optimal domain width is at much smaller domain thicknesses and is not within the range of displayed results). Indeed, for perpendicularly oriented donors, increasing the anisotropy is expected to enhance the exciton transport to the interface in such a way that the decay length becomes anisotropic and considerably enhanced in the direction perpendicular to the donor−acceptor interfaces. As discussed earlier, the exciton decay length l_D correlates with the optimal domain widths, thereby rationalizing our results.

IV. Summary and Outlook

In this research, we developed a model to understand the photovoltaic properties for polymer devices which consider as input the density and orientational ordering in donor and acceptor phases. This model improves upon the previous work by taking into account the anisotropic nature of charge transport in conjugated polymers. Our study focuses on self-assembly in rod−coil block copolymers as means to achieve desirable values of photovoltaic efficiency. Rod−coil block copolymers derive their advantages from their ability to form microphase-separated

morphologies and the capability for the rodlike units to be orientationally ordered. The perpendicularly oriented lamellar morphology was shown to be the most desirable morphology for obtaining high values of photocurrent. Also, the other factors that can improve the photovoltaic efficiency were a stronger degree of chemical incompatibility between the donor and acceptor units and higher value of orientational order parameter. Such conditions lead to a well-segregated microphase structure of rod−coil block copolymers having perfectly aligned rod molecules. Within these morphologies we demonstrated that an optimal domain spacing and optimal degree of anisotropy leads to the highest efficiencies.

Our model can be utilized to study other systems being considered for polymer solar cell devices like blends of conjugated molecules with fullerene derivatives.[1,14] Our model provides the framework to calculate photovoltaic behavior ($J-V$ curve) once the density of species and orientational ordering of conjugated molecules are known. Our future studies will address similar issues in the context of models for such donor−acceptor blends.

Acknowledgment. This work was supported in part by a grant from Robert A. Welch Foundation though (F-1599) and the National Science Foundation grant 0730243. We thank Profs. Nigel Clarke and Rachel Segalman and Dr. Victor Pryamitsyn for insightful comments and discussions. The authors acknowledge the use of computer resources at Texas Advanced Computing Center (TACC) for the calculations reported in this article.

References and Notes

(1) Coakley, K.; McGehee, M. *Chem. Mater.* **2004**, *16*, 4533–4542.
(2) Mayer, A. C.; Scully, S. R.; Hardin, B. E.; Rowell, M. W.; McGehee, M. D. *Mater. Today* **2007**, *10*, 28–33.
(3) Buxton, G. A.; Clarke, N. *Modell. Simul. Mater. Sci. Eng.* **2007**, *15*, 13–26.
(4) Sariciftci, N. S.; Smilowitz, L.; Heeger, A. J.; Wudl, F. *Science* **1992**, *258*, 1474–1476.
(5) Lei, B.; Yao, Y.; Kumar, A.; Yang, Y.; Ozolins, V. *J. Appl. Phys.* **2008**, *104*, 024504.
(6) Mihailetchi, V. D.; Koster, L. J. A.; Hummelen, J. C.; Blom, P. W. M. *Phys. Rev. Lett.* **2004**, *93*, 216601.
(7) Tao, Y.; McCulloch, B.; Kim, S.; Segalman, R. *Soft Matter*, accepted, 2009.
(8) Segalman, R. A.; Brochon, C.; Hadziioannou, G. *Organic Photovoltaics: Mechanisms, Materials and Devices*; Marcel Dekker: New York, 2005.
(9) Tang, C. W. *Appl. Phys. Lett.* **1986**, *48*, 183–185.
(10) Barker, J. A.; Ramsdale, C. M.; Greenham, N. C. *Phys. Rev. B* **2003**, *67*, 075205.
(11) Blom, P.; Mihailetchi, V.; Koster, L.; Markov, D. *Adv. Mater.* **2007**, *19*, 1551–1566.
(12) Buxton, G. A.; Clarke, N. *Phys. Rev. B* **2006**, *74*, 085207.
(13) Dennler, G.; Scharber, M. C.; Brabec, C. J. *Adv. Mater.* **2009**, *21*, 1323–1338.
(14) Shaheen, S. E.; Brabec, C. J.; Sariciftci, N. S.; Padinger, F.; Fromherz, T.; Hummelen, J. C. *Appl. Phys. Lett.* **2001**, *78*, 841–843.
(15) Yu, G.; Gao, J.; Hummelen, J. C.; Wudl, F.; Heeger, A. J. *Science* **1995**, *270*, 1789−1791.
(16) Huynh, W.; Dittmer, J.; Libby, W.; Whiting, G.; Alivisatos, A. *Adv. Funct. Mater.* **2003**, *13*, 73–79.
(17) Huynh, W. U.; Dittmer, J. J.; Alivisatos, A. P. *Science* **2002**, *295*, 2425−2427.
(18) de Boer, B.; Stalmach, U.; van Hutten, P. F.; Melzer, C.; Krasnikov, V. V.; Hadziioannou, G. *Polymer* **2001**, *42*, 9097–9109.
(19) Hadziioannou, G. *MRS Bull.* **2002**, *27*, 456–460.
(20) Lindner, S.; Thelakkat, M. *Macromolecules* **2004**, *37*, 8832–8835.
(21) Barrau, S.; Heiser, T.; Richard, F.; Brochon, C.; Ngov, C.; van de Wetering, K.; Hadziioannou, G.; Anokhin, D. V.; Ivanov, D. A. *Macromolecules* **2008**, *41*, 2701–2710.
(22) Park, S. H.; Roy, A.; Beaupre, S.; Cho, S.; Coates, N.; Moon, J. S.; Moses, D.; Leclerc, M.; Lee, K.; Heeger, A. J. *Nat. Photonics* **2009**, *3*, 297–302.
(23) Tao, Y.; Ma, B.; Segalman, R. A. *Macromolecules* **2008**, *41*, 7152–7159.
(24) Pryamitsyn, V.; Ganesan, V. *J. Chem. Phys.* **2004**, *120*, 5824–5838.
(25) Matsen, M.; Barrett, C. *J. Chem. Phys.* **1998**, *109*, 4108–4118.
(26) Reenders, M.; ten Brinke, G. *Macromolecules* **2002**, *35*, 3266–3280.
(27) Chen, J. T.; Thomas, E. L.; Ober, C. K.; Mao, G.-p. *Science* **1996**, *273*, 343–346.
(28) Olsen, B.; Li, X.; Wang, J.; Segalman, R. *Macromolecules* **2007**, *40*, 3287–3295.
(29) Olsen, B.; Segalman, R. *Macromolecules* **2005**, *38*, 10127–10137.
(30) Radzilowski, L. H.; Carragher, B. O.; Stupp, S. I. *Macromolecules* **1997**, *30*, 2110–2119.
(31) Olsen, B.; Segalman, R. *Macromolecules* **2006**, *39*, 7078–7083.
(32) Shah, M.; Pryamitsyn, V.; Ganesan, V. Unpublished, **2009**.
(33) Koster, L. J. A.; Smits, E. C. P.; Mihailetchi, V. D.; Blom, P. W. M. *Phys. Rev. B* **2005**, *72*, 085205.
(34) Coakley, K.; Srinivasan, B.; Ziebarth, J.; Goh, C.; Liu, Y.; McGehee, M. *Adv. Funct. Mater.* **2005**, *15*, 1927–1932.
(35) Collini, E.; Scholes, G. D. *Science* **2009**, *323*, 369–373.
(36) Bredas, J.-L.; Silbey, R. *Science* **2009**, *323*, 348–349.
(37) Erb, T.; Zhokhavets, U.; Gobsch, G.; Raleva, S.; Stühn, B.; Schilinsky, P.; Waldauf, C.; Brabec, C. *Adv. Funct. Mater.* **2005**, *15*, 1193–1196.
(38) Baek, W.-H.; Yang, H.; Yoon, T.-S.; Kang, C.; Lee, H. H.; Kim, Y.-S. *Sol. Energy Mater. Sol. Cells* **2009**, *93*, 1263–1267.
(39) Sirringhaus, H.; Brown, P. J.; Friend, R. H.; Nielsen, M. M.; Bechgaard, K.; Langeveld-Voss, B. M. W.; Spiering, A. J. H.; Janssen, R. A. J.; Meijer, E. W.; Herwig, P.; de Leeuw, D. M. *Nature* **1999**, *401*, 685–688.
(40) Kinder, L.; Kanicki, J.; Petroff, P. *Synth. Met.* **2004**, *146*, 181–185.
(41) Lan, Y.-K.; Huang, C.-I. *J. Phys. Chem. B* **2008**, *112*, 14857–14862.
(42) Selberherr, S. *Analysis and Simulation of Semiconductor Devices*; Springer: New York, 1984.
(43) Shah, M.; Pryamitsyn, V.; Ganesan, V. *Appl. Phys. Lett.* **2009**, *95*, 194101−194103.
(44) Fahrenbruch, A.; Bube, R. *Fundamentals of Solar Cells*; Academic Press: New York, 1983.
(45) Onsager, L. *Phys. Rev.* **1938**, *54*, 554–557.
(46) Braun, C. L. *J. Chem. Phys.* **1984**, *80*, 4157–4161.
(47) Blom, P. W. M.; de Jong, M. J. M.; Breedijk, S. *Appl. Phys. Lett.* **1997**, *71*, 930–932.
(48) Shah, M.; Pryamitsyn, V.; Ganesan, V. *Macromolecules* **2008**, *41*, 218–229.
(49) de Gennes, P. G. *The Physics of the Liquid Crystals*; Oxford University Press: New York, 1974.
(50) Lacic, S.; Inganas, O. *J. Appl. Phys.* **2005**, *97*, 124901.
(51) Scott, J. C.; Malliaras, G. G. *Chem. Phys. Lett.* **1999**, *299*, 115–119.
(52) Scharfetter, D.; Gummel, H. *IEEE Trans. Electron Devices* **1969**, *16*, 64–77.
(53) Press, W.; Teukolsky, S.; Vetterling, W.; Flannery, B. *Numerical Recipes in Fortran*; Cambridge University Press: Cambridge, 1992.
(54) Matsen, M. W. *J. Chem. Phys.* **1997**, *106*, 7781–7791.
(55) Olsen, B. D.; Shah, M.; Ganesan, V.; Segalman, R. A. *Macromolecules* **2008**, *41*, 6809–6817.
(56) Gupta, D.; Bag, M.; Narayana, K. S. *Appl. Phys. Lett.* **2008**, 92.
(57) Kim, M.-S.; Kim, B.-G.; Kim, J. *ACS Appl. Mater. Interfaces* **2009**, *1*, 1264–1269.